SAND2019-6609C

Dynamic Temperature-Dependent Tensile Behavior of Soft Ferromagnetic Alloy Fe-Co-2V

Brett Sanborn*[1], *Bo* Song[1], *Don* Susan[1], *Kyle* Johnson[1], *Jeff* Dabling[1], *Jay* Carroll[1], *Adam* Brink[1], *Scott* Grutzik[1], and *Andrew* Kustas[1]

[1]Sandia National Laboratories, 1515 Eubank SE, Albuquerque, NM 87108 USA

Abstract. Fe-Co-2V is a soft ferromagnetic alloy used in electromagnetic applications due to excellent magnetic properties. However, the discontinuous yielding (Lüders bands), grain-size-dependent properties (Hall-Petch behavior), and the degree of order/disorder in the Fe-Co-2V alloy makes it difficult to predict the mechanical performance, particularly in abnormal environments such as elevated strain rates, high/low temperatures, and combinations of these. Thus, experimental characterization of the high-strain-rate stress-strain properties of the Fe-Co-2V alloy at high/low temperatures is desired, which are used for material model development in numerical simulations. In this study, the high-rate tensile response of Fe-Co-2V is investigated with a pulse-shaped Kolsky tension bar from cold to hot temperatures. Effect of temperature on yield stress, ultimate tensile stress, and elongation to failure are discussed.

1 Introduction

Applications such as magnetic bearings and rotors require soft ferromagnetic alloys such as Fe-Co-2V because of their high magnetic saturation. During the applications, soft ferromagnetic alloys may be required to bear sufficient mechanical loads under a wide range of environments, such as extreme ranges of temperature and loading rate. Currently, limited studies are available regarding the mechanical response of Fe-Co-2V alloys, with most focusing on the response under elevated temperatures. Ren et al. measured the tensile stress-strain response of Fe-Co-2V over a temperature range from ambient to 800°C [1]. Ren et al. found that the Fe-Co-2V displayed a linear elastic response, followed by a Lüders band (flat plateau) before linearly work hardening until failure. Below about 300°C, Ren et al. [1] found that the yield strength decreased with increasing temperature. The decrease in yield strength became insignificant when the temperature was between 300-700°C. Grain size within the material affected the yield strength and followed a Hall-Petch relationship [1]. Duckham et al. investigated Fe-Co-2V over a wide range of grain sizes and temperatures ranging from ambient to 500°C [2]. Their study reinforced the assertion that the Fe-Co-2V followed a Hall-Petch relationship between yield stress and grain diameter and added that both ordered and disordered Fe-Co-2V followed the same relationship. In terms of temperature, Duckham et al. [2] also concurred that the yield stress decreased with increasing temperature. The work hardening rate of the material with grain sizes between 100-150 nm was found to be fairly constant at temperatures up to approximately 300°C, but the material with grain sizes of 290 nm experienced a decrease in hardening rate when the temperature was elevated only to 100°C.

All the available studies have presented the tensile properties of Fe-Co-2V alloys at elevated temperatures but were limited to quasi-static strain rates. Ren et al. did vary the strain rate within the quasi-static regime and discovered a strain rate effect [1]. No information is available on the stress-strain relationship at high strain rates. Furthermore, no investigation has been undertaken to study Fe-Co-2V at low temperatures. Such high-rate, high- or low-temperature material property information of the Fe-Co-2V is critical for the performance assessment under abnormal extreme environments to which materials in magnetic applications may be exposed.

In this study, we use a Kolsky tension bar with an environmental chamber to simultaneously subject the Fe-Co-2V alloy to both extreme temperatures from -100 to 100°C and a high strain rate of 230 s^{-1}. Effects of temperature on yield stress, flow stress, and ductility are explored.

* Corresponding author: bsanbor@sandia.gov

2 Materials and Methods

The Fe-Co-2V alloy studied was manufactured by Metal Werks Inc. Dog-bone tensile specimens were machined with the geometry shown in Fig. 1. Dynamic tensile experiments were conducted at temperatures of -100, -50, 23, and 100°C. The strain rate was held constant at approximately 230 s^{-1} for all experiments to determine the temperature effect. Five experiments were conducted at each temperature condition.

Fig. 1. Specimen Design

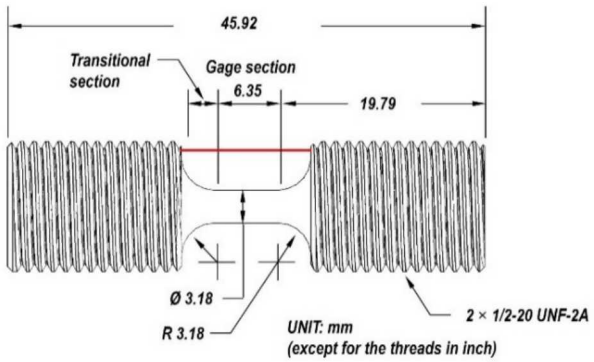

A Kolsky tension bar as shown in Fig. 2 was used for dynamic tensile experiments. The incident and transmission bars were 3.66 and 2.13 m long, respectively, and were made of C300 maraging steel. In this configuration, a solid cylindrical striker is contained inside the gun barrel [3]. When the striker is launched by releasing compressed gas from the cylinder, the striker is propelled toward the opposite end of the gun barrel and strikes an end cap. The generated tensile wave travels through the gun barrel and into the incident bar through a coupler. The tensile wave then propagates along the incident bar until it reaches the specimen which is threaded into the incident and transmission bars and locked into place using two lock nuts. While the specimen is being loaded in dynamic tension, part of the incident pulse is reflected into the incident bar as a reflected pulse, and part of the pulse is transmitted into the transmission bar. The primary benefit of a Kolsky tension bar with this design is that traditional pulse shaping techniques for general dynamic compression tests are easily implemented for dynamic tensile tests. In this study, annealed C11000 copper disks were placed on the inside of the end cap as pulse shapers. Like compression experiments, the dimensions of the pulse shaper can be changed to tailor the profile of the loading pulse for different temperature conditions.

For experiments at high and low temperatures, an environmental chamber was installed at the specimen location to locally heat or cool the specimen and bar ends. A thermocouple was placed on the bar a few centimeters away from the sample. The temperature of the bar and the specimen was assumed to be equilibrated. The material properties of the bars were assumed to be constant within the temperature range (-100 to 100 °C) investigated in this study.

At ambient temperatures, the specimen strain was measured using a linear laser and detector configuration. Shown in Fig. 2a, this configuration used a single beam laser split into two separate high-speed photodetectors using a mirror prism [4]. This allowed displacements of the incident (L_1) and transmission (L_2) bars to be tracked independently during the experiment to calculate the strain history of the specimen. The laser measurement eliminates the possible error in specimen displacement measurement with a traditional method using strain gage signals due to wave reflection at the complicated interfaces, i.e., threads, between the specimen and the bars. However, a previous study showed that when sufficient torque is applied to the lock nuts experimental error is minimal when stain gage signals were used to calculate the displacements at both ends of the specimen [5]. For the experiments where the thermal chamber was used (Fig. 2b), using the laser system was not possible. With proper torque applied to the lock nuts, the specimen strain was therefore calculated using the strain gage signal

$$L_1 - L_2 = \Delta L = C_0 \cdot \int_0^t \left(\varepsilon_i(t) - \varepsilon_r(t) - \varepsilon_t(t)\right) dt \qquad (1)$$

where C_0 is the bar wave speed and ε_i, ε_r, and ε_t are incident, reflected, and transmission bar strains, respectively.

Fig. 2. a) Kolsky tension bar for ambient temperatures. b) Kolsky bar for high and low temperatures

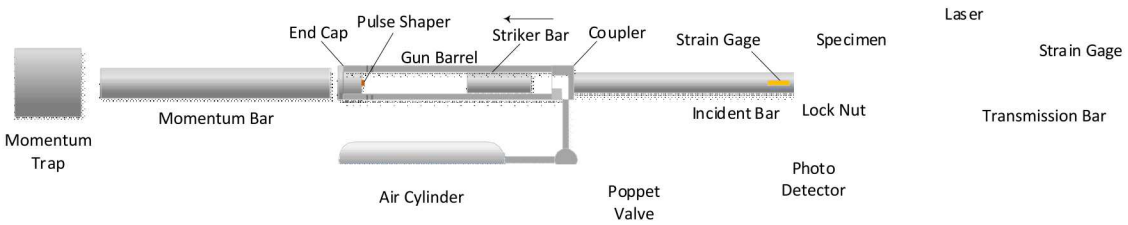

a)

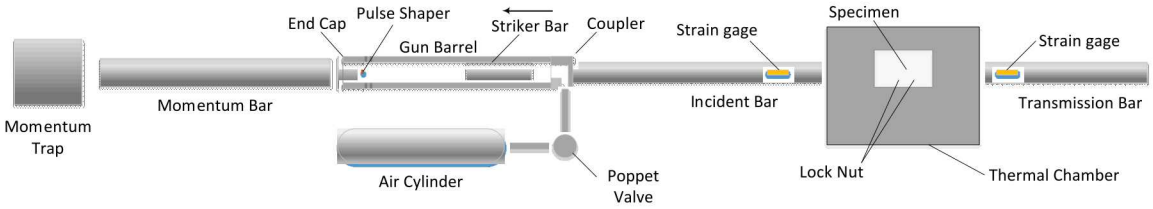

b)

For either the laser or strain gage strain measurements, the deformation of both the gage and non-gage sections were recorded. Thus, the specimen strain must be corrected to include only the gage section. Because the Fe-Co-2V material has an elastic, followed by linear hardening behavior, the specimen strain correction method developed by Song et al. [6] is applicable to correct the specimen strain. Details of the linear hardening strain correction method were presented in [6], however, the general method is summarized here. The correction method divides the stress-strain curve into four regions, shown in Fig. 3.

Fig. 3. Idealized linear elastic, work hardening material [6].

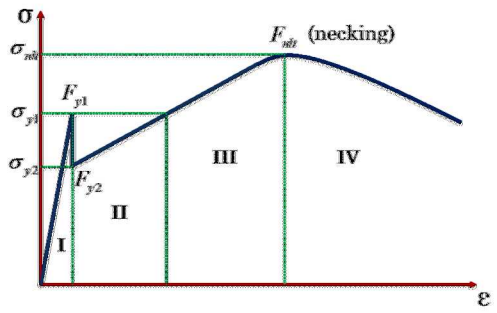

In Fig. 3, σ_{y1} and σ_{y2} are the upper and lower yield strengths, and σ_{ult} is the ultimate tensile strength. Forces F_{y1}, F_{y2}, and F_{ult} correspond to upper yield, lower yield, and onset of necking. As will be shown later, the Fe-Co-2V specimens only require use of Regions I-III since no necking occurs. The specimen strain is calculated using Regions I-III from with the piecewise function [6],

$$\varepsilon = \begin{cases} c' \cdot \dfrac{\Delta L}{L_s} & \left(\text{Region I}\ \ \sigma < \sigma_{y1}\right) \\ \dfrac{\Delta L}{L_s} - \dfrac{F}{M} \cdot \left(\dfrac{1}{c'} - 1\right) & \left(\text{Region II}\ \ \sigma_{y2} < \sigma < \sigma_{y1}\right) \\ \dfrac{\dfrac{F_{y1}}{M} + \Delta L - \dfrac{2 \cdot F}{E_s \cdot \pi} \cdot \int_{x_0}^{x_l} \dfrac{dx}{R_Q} - \dfrac{F_{y1}}{M} \cdot (2x_0 + L_s)}{\dfrac{2 \cdot F \cdot r_0^2 \cdot \int_0^{x_0} \dfrac{dx}{R_Q} - 2 \cdot F_{y2} \cdot x_0}{F - F_{y2}} + L_s} & \left(\text{Region III}\ \ \sigma > \sigma_{y1}\right) \end{cases} \quad (2)$$

R_Q and M are defined as

$$R_Q = \left(R + r_0 - \sqrt{R^2 - x^2}\right)^2 \quad (3)$$

$$M = E_s \cdot \pi \cdot r_0^2 \quad (4)$$

Where R and r_0 are the radii of the shoulder and gage sections of the specimen, respectively. For the geometry used in this study, $x_1 = R = r_0 = 3.18$ mm. L_s is the length of the straight gage section, and F is the force generated by the specimen as a function of time. The specimen Young's modulus is denoted E_s, while c' is a constant also derived from the specimen geometry,

$$c' = \frac{1}{1 + 2 \cdot \dfrac{r_0^2}{L_s} \cdot \int_0^{x_l} \dfrac{dx}{R_Q}} \quad (5)$$

The elastic/plastic boundary, x_0, increases with increasing applied force, F,

$$x_0 = r_0 \sqrt{\left(\sqrt{\frac{F}{F_{y1}}} - 1\right) \cdot \left[2 \cdot \frac{R}{r_0} - \left(\sqrt{\frac{F}{F_{y1}}} - 1\right)\right]} \quad (6)$$

The specimen stress history was calculated using

$$\sigma(t) = E_0 \cdot \varepsilon_t(t) \cdot \frac{A_0}{A_s} \quad (7)$$

where E_0 is the Young's modulus of the bar, A_0 is the bar cross-sectional area, and A_s is the specimen cross-sectional area.

3 Results and Discussion

A typical set of strain signals from a Kolsky tension bar experiment on Fe-Co-2V alloy are shown in Fig. 4. Figure 4 shows a uniquely-shaped incident pulse compared to most Kolsky bar experiments. Achieved through pulse shaping, this nearly linear hardening incident pulse was required to deform the specimen at a near constant strain rate, rather than the usual trapezoidal incident pulse. The specimen response shown in Fig. 4 displays high and low yield stresses followed by linear hardening until abrupt failure. The corresponding displacements of the incident and transmission bar ends are shown in Fig. 5.

Fig. 4. Original experimental record for Fe-Co-2V under dynamic tension

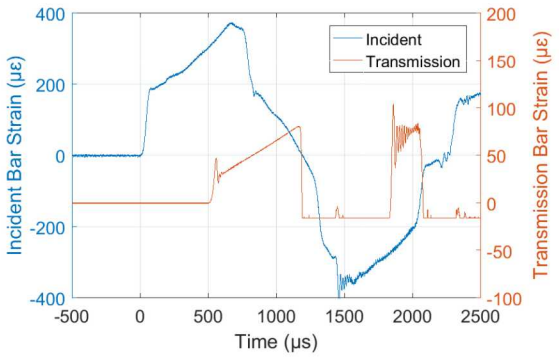

Fig. 5. Displacement history

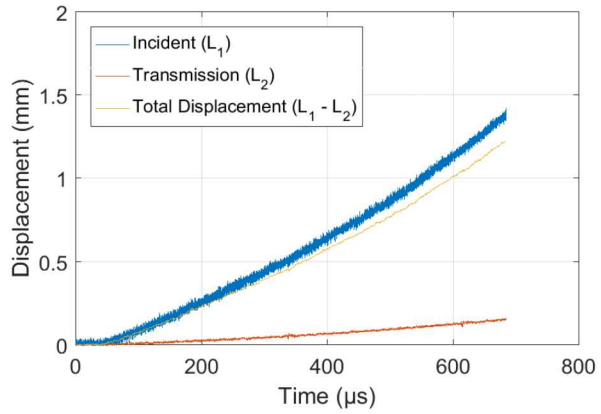

Using the displacement histories in Fig. 5, the linear hardening strain correction method of Song et al. [6] was applied to calculate strain and strain rate histories, the results of which are shown in Fig. 6. In this case, the specimen was subjected to a nearly constant strain rate of approximately 230 s^{-1}, which was achieved through pulse shaping. At an engineering strain of approximately 5%, a decrease in strain rate was observed which was caused by the beginning of plastic deformation in the shoulders of the specimen, after which the strain rate returned to a similar level [6].

Overall, the general shape of the stress-strain curve at high rate is like the quasi-static behavior, but some differences are noticeable. The dynamic stress-strain curve has a distinct upper and lower yield response prior to onset of linear hardening. This contrasts with the quasi-static case where yield occurred, followed by a flat plateau (Lüders banding) prior to hardening [1,2].

Fig. 6. Engineering stress-strain and strain rate behavior of Fe-Co-2V at 23°C

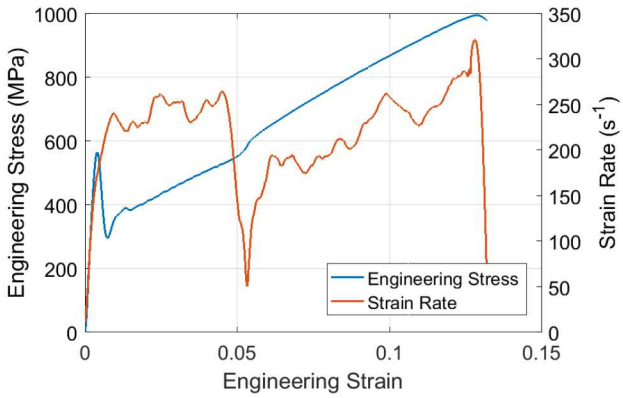

Using the same process, the temperature of the thermal chamber was varied from -100 to 100°C. The strain rate was held constant at approximately 230 s^{-1} for all experiments. The average engineering stress-strain curves are shown in Fig. 7, which represent an average of five experiments under each condition. Notably, both the high and low yield stresses increased with decreasing temperature. The rate of hardening was independent of temperature. The behavior at ambient temperature and 100°C was nearly identical, but higher strain to failure and ultimate stress was observed at 100°C.

Fig. 7. Temperature effect on stress-strain behavior of Fe-Co-2V. Averaged curves at 230 s^{-1}

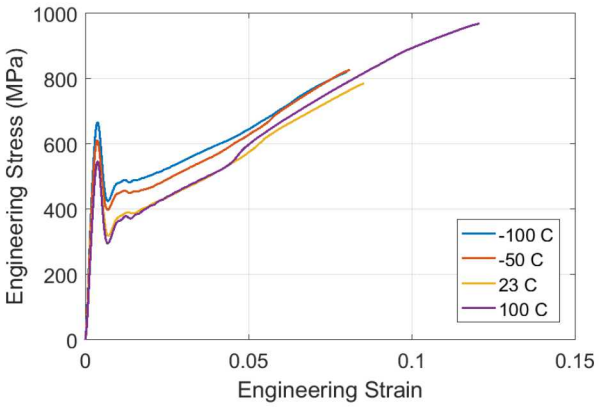

Further temperature effects are shown in Fig. 8 at different strains. As was noted earlier, the yield stress was the highest at -100°C and decreased with increasing temperature. The flow stresses at both 3% and 6% strains were also the highest at -100°C and decreased with increasing temperature. The ultimate tensile stress showed the opposite trend where the average value at 100°C was about 24% higher than at -100°C. This is most likely linked to the increase in overall ductility with increasing temperature, which is shown in Fig. 9. The Fe-Co-2V had 65% higher average failure strain at 100°C compared to -100°C.

Fig. 8. Temperature effects on yield, flow, and ultimate stress. Error bars represent one standard deviation.

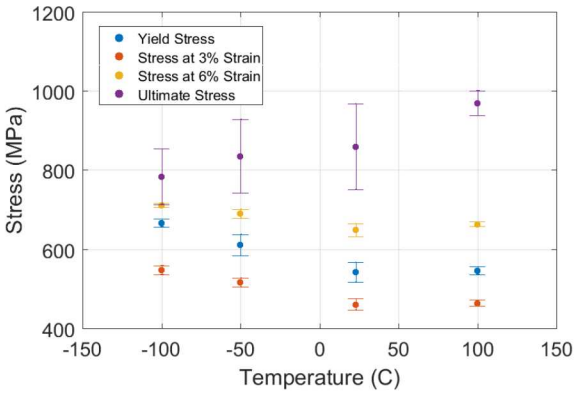

Fig. 9. Temperature effect on failure strain. Error bars represent one standard deviation.

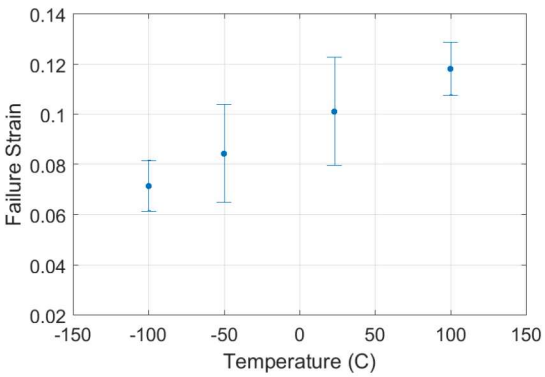

Comparisons of these results to any literature data are difficult to make since to our knowledge, no studies are available to address temperature effects over this range for Fe-Co-2V. Duckham et al. [2] investigated a similar Fe-Co-V alloy under quasi-static tension but mainly looked at the elevated temperature behavior. In general, the behavior found in this study at ambient temperature and 100°C agrees with Duckham et al. [2], where only a minor difference was measured over that temperature range. Duckham et al. similarly noted that the hardening rate of the tensile stress-strain curve did not change with temperature until the temperature reached about 300°C, though this was a grain size dependent relationship.

Though temperature-dependent behavior of Fe-Co-2V is sparse in the literature, the tensile stress-strain behavior of a few different steel types has been studied at cold temperatures which may be used for rough comparison. The temperature effect measured here for Fe-Co-2V is somewhat less dramatic compared to 304 stainless steel. Zheng and Yu saw an increase in ultimate stress of 304 stainless steel by about 24%, under quasi-static conditions when the temperature was dropped from 27°C to -100°C [7]. The ultimate strain was also about 40% lower at -100°C compared to 27°C [7]. Another quasi-static study on mild and high-strength S690 steels showed similar behavior from 30°C to -80°C [8]. Yan et al. [8] found that the mild steel had approximately 18% higher ultimate tensile strength at low temperature while the high-strength steel was only about 9% stronger at low temperature. Unlike the Fe-Co-2V alloy, the failure strain of both types of steel remained relatively constant over the temperature range [8].

Post-test failure analysis of the Fe-Co-2V samples showed that the material underwent brittle fracture. This was observed in all cases regardless of temperature. Each of the specimens failed within the gage section, but no necking was noticeable in any case. This agrees with the stress-strain behavior shown in Fig 5, since no localized necking was observed prior to fracture.

4 Conclusion

A Kolsky tension bar with an environmental chamber was used to measure the temperature dependent properties of the soft ferromagnetic alloy Fe-Co-2V at high strain rate. A specimen strain correction was applied to the measured displacement data to accurately calculate the strain over the gage section. Tensile stress-strain curves were presented for temperatures of -100, -50, 23, and 100°C at the same strain rate of 230 s^{-1}.

Overall, the dynamic tensile stress-strain behavior was similar over the temperature range. The flat Lüders band plateau usually seen for this material at quasi-static strain rates was absent at high rate. Instead, the material displayed a high and low yield behavior prior to hardening. Notably, the post-yield hardening rate remained constant despite varying the temperature. In general, the upper yield stress and flow stresses at the same strain levels increased with decreasing temperature. An opposite effect was observed for ultimate stress wherein the ultimate stress increased with increasing temperature. This is most likely due to the higher ductility at higher temperatures.

In all cases, the material underwent brittle fracture at high strain rate. Each of the specimens failed within the gage section but maintained a circular cross section with no signs of necking.

This study serves as a first look into the dynamic temperature dependent tensile properties of soft ferromagnetic alloys such as Fe-Co-2V.

Sandia National Laboratories is a multimission laboratory managed and operated by National Technology and Engineering Solutions of Sandia, LLC, a wholly owned subsidiary of Honeywell International, Inc., for the U.S. Department of Energy's National Nuclear Security Administration under contract DE-NA0003525. The views expressed in the article do not necessarily represent the views of the U.S. Department of Energy or the United States Government.

References

1. L. Ren, S. Basu, R.H. Yu, A. Parvizi-Majidi, J. Mater. Sci. **36**, (2001)
2. A. Duckham, D.Z. Shang, D. Liang, V. Luzin, R.C. Cammarata, R.L Leheny, C.L. Chien, T.P. Weihs, A. Mater. **51**, (2003)
3. B. Song, B.R. Antoun, K. Connelly, J. Korellis, W.Y. Lu, Meas. Sci. Technol. **22** (2011)
4. X. Nie, B. Song, C.M Loeffler, J. Dyn. Behav. Mater. **1**, (2015)
5. Y. Qiu, C.M. Loeffler, X. Nie, B. Song, Meas. Sci. Technol. **29,** (2018)
6. B. Song, B. Sanborn, D. Susa, K. Johnson, J. Dabling, J. Carroll. A. Brink, S. Grutzik, A. Kustas. Int. J. Impact. Eng. (submitted 2019)
7. C. Zheng, W. Yu, Mater. Sci. Eng. A, **710** (2018)
8. J.B. Yan, J.Y.R. Liew, M.H. Zhang, J.Y. Wang. Mater. Des. **61**, (2014)